

Narrow optical transitions in erbium-implanted silicon waveguides

Andreas Gritsch,* Lorenz Weiss,* Johannes Früh, Stephan Rinner, and Andreas Reiserer†

*Quantum Networks Group, Max-Planck-Institut für Quantenoptik,
Hans-Kopfermann-Strasse 1, D-85748 Garching, Germany and*

*Munich Center for Quantum Science and Technology (MCQST), Ludwig-Maximilians-Universität München,
Fakultät für Physik, Schellingstr. 4, D-80799 München, Germany*

The realization of a scalable architecture for quantum information processing is a major challenge of quantum science. A promising approach is based on emitters in nanostructures that are coupled by light. Here, we show that erbium dopants in high-purity silicon-on-insulator chips combine the ease of low-loss waveguide fabrication with < 1 GHz inhomogeneous broadening, strong optical transitions, and an outstanding optical coherence even at temperatures of 8 K, with an upper bound to the homogeneous linewidth of ~ 20 kHz. Our study thus introduces a promising materials platform for the implementation of on-chip quantum memories, microwave-to-optical conversion, and distributed quantum information processing.

Individual dopants in solids are prime candidates for the realization of quantum computers [1] and quantum networks [2, 3]. While a large variety of host materials is explored [4], the use of silicon seems particularly attractive: First, nanofabrication has reached a unique level of maturity in this material. Second, a platform for integrated photonic processing, both classical [5] and quantum [6], is readily available. Finally, defect-free and isotopically purified crystalline layers can be obtained on a wafer-scale [7], which can largely eliminate the decoherence via nuclear spins and paramagnetic impurities [8] and reduce the inhomogeneous broadening of optical transitions [9].

To harness the mentioned advantages for quantum applications, different emitters in silicon have been explored [9–12], and single dopants have been detected optically [13–15]. Among these emitters, and also those in all other host materials [4], erbium stands out since it offers an optical transition with lifetime-limited coherence [16] in the main wavelength band of telecommunication, where loss in optical fibers is minimal. In addition, the narrow linewidth of erbium dopants eliminates the requirement of single-defect positioning encountered with other emitters [3], and offers unique potential for spectrally multiplexed single-qubit control [17].

In recent experiments, erbium has been integrated into nanophotonic silicon waveguides with inhomogeneous broadening of ~ 1 GHz and a homogeneous linewidth $\lesssim 0.1$ GHz [11]. Here, we show that by optimizing the implantation conditions and by using high-purity silicon-on-insulator samples, grown by chemical vapor deposition (CVD), we can achieve erbium integration in new sites that exhibit strongly improved properties. In particular, we observe the fastest optical transitions of erbium dopants in any known host material, and exceptionally large crystal-field splittings, which leads to low Orbach decoherence and thus enables narrow homogeneous linewidths < 20 kHz up to a temperature of 8 K, which is conveniently accessible with dry ^4He cryocoolers. These improvements pave the way for using erbium-implanted

silicon for quantum applications.

To achieve narrow optical transitions, one has to ensure that the silicon host material is single-crystalline and has a low concentration of defects and impurities. In this context, standard silicon-on-insulator (SOI) wafer fabrication, e.g. via the smart-cut technique, involves detrimental techniques such as ion implantation and chemo-mechanical polishing [5]. We therefore implemented an alternative approach to obtain high-purity crystalline layers. The procedure starts with a commercial SOI wafer that is thinned down to ~ 0.05 μm before a ~ 0.14 μm thick epitaxial layer of pure silicon with natural isotope abundance is grown by CVD. Subsequently, erbium is implanted with a total dose of $2.9 \cdot 10^{12}$ cm^{-2} in two steps with energies of 0.1 MeV and 0.35 MeV. Thus, we expect an approximately homogeneous dopant concentration of 10^{17} cm^{-3} , comparable to that in [11], in the center region of the waveguide.

In contrast to previous works [11, 13, 18, 19], no post-implantation thermal treatment is applied. Instead, the doping process is performed at a temperature of ~ 800 K, hot enough to directly repair the implantation damage but cold enough to largely prevent erbium segregation [19]. The wafers are then diced and 0.7 μm wide rectangular waveguides are fabricated by electron-beam lithography and reactive ion etching in fluorine chemistry. A cross section of the device is shown in Fig. 1a (inset). Similar to previous work [18], we find a slightly increased but still moderate loss of (5.7 ± 1.2) dB/cm in erbium-implanted as compared to (3.5 ± 1.2) dB/cm in undoped waveguides. Further details about the sample fabrication and characterization are provided in the supporting material.

To achieve a strong signal, we use several mm long waveguides, which are coupled to a tapered single-mode optical fiber with an efficiency of up to 0.3. The sample is mounted in a closed-cycle cryostat at < 2 K, where resonant fluorescence spectroscopy reveals the wavelengths at which the implanted dopants can be excited. The transitions between the lowest crystal field levels of the inner

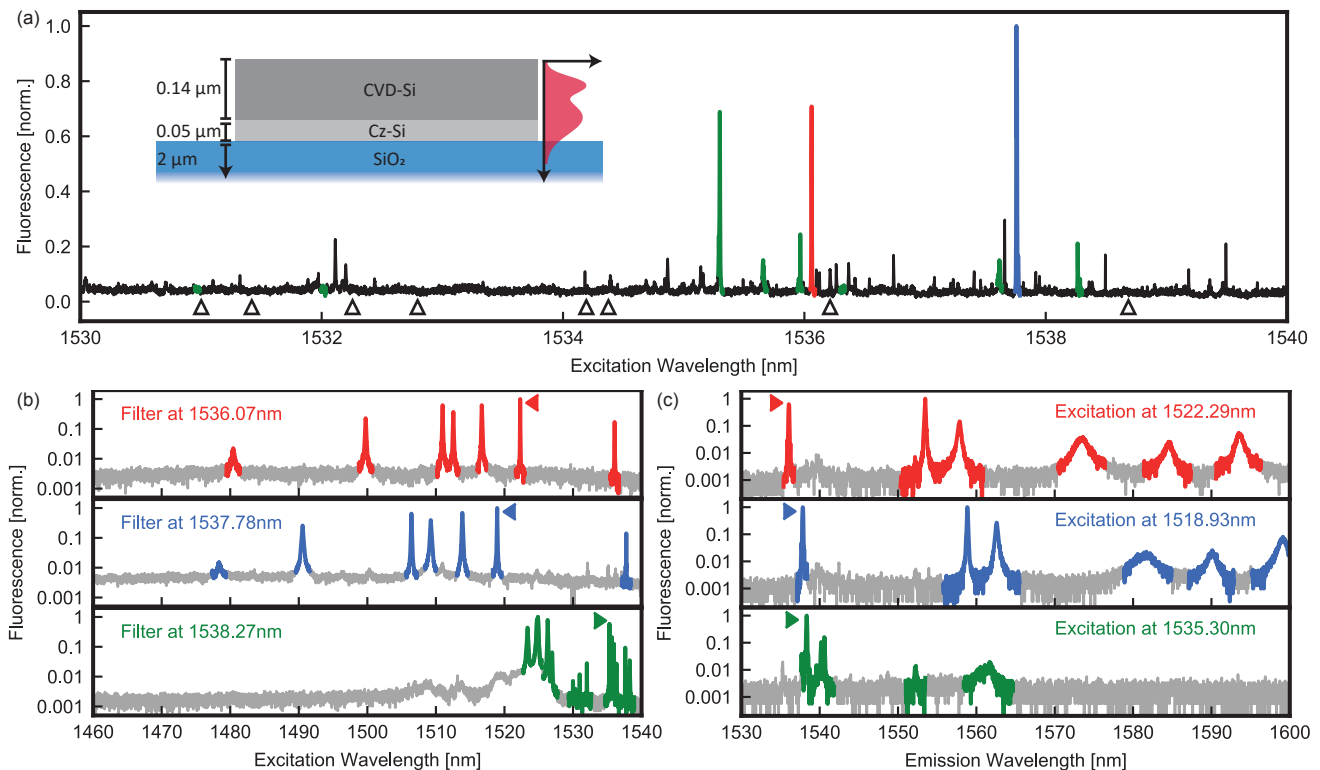


FIG. 1. **Spectroscopy of erbium-implanted silicon waveguides.** (a) Inset: Sample geometry. The $0.7\ \mu\text{m}$ wide silicon waveguide resides on a buried oxide layer (blue). It consists of a bottom layer (light grey) of Cz-material, on which a high-purity silicon layer (dark grey) has been grown by chemical vapor deposition. Implantation with two different energies gives two peaks in the expected erbium density (red). Main graph: Scanning the excitation laser frequency reveals several narrow fluorescence peaks. The position of the brightest lines differs from that found in a previous experiment with a different sample preparation [11] (black open triangles). (b) Insertion of a narrowband optical filter, tuned on resonance with one of the three most prominent peaks (color coding), eliminates the broadband background and reveals the excited state crystal fields of the individual sites. (c) Keeping the laser on resonance with one of the main peaks while scanning the filter gives the ground state crystal fields. The filled triangles in c(b) mark the filter (excitation laser) position in b(c).

4f-shell of erbium occur between 1530 and 1540 nm [20]. Similar to our previous work [11], we find several narrow emission lines in this range. However, their position is different, as shown in Fig. 1a. The shift is too large to be caused by strain [21]. We therefore conclude that owing to the changed sample preparation technique, erbium is integrated at different sites in the high-purity crystalline layer studied in this work. In the following, we show that two of the new sites with the strongest signal also have very favorable properties for quantum applications.

In rare-earth doped crystals, the transition strength and optical coherence depend on the splitting of the 4f levels by the crystal field (CF) [20]. To determine this splitting, we insert a tunable and narrowband optical filter into the detection path. We first keep the filter resonant with one of the brightest peaks in the above measurement and scan the excitation laser to shorter wavelengths. As can be seen in Fig. 1b, we can thus identify the higher lying CF levels in the optically excited state manifold. We then keep the laser at the brightest peak and scan the filter frequency to determine the energy lev-

els in the ground state CF manifold, see Fig. 1c. The high signal-to-noise ratio enabled by our low-loss waveguides ensures that all levels that are in reach of the laser and filter are observed.

Assigning the observed peaks in all measurements, we find that erbium is integrated at several different sites in our structures. At least one of them is "optically active" [19], which means that it can be excited by electrons in the conduction band. We therefore detect fluorescence of this site "O" independent of the excitation wavelength provided the power is large enough to give a significant above-bandgap excitation (see supporting information). While optical activity is key to the realization of electrically-driven photon emission and lasing [19], it is not required for quantum applications, and may even be detrimental to the optical coherence. Therefore, we focus on the three bright sites which are not coupled to the conduction band (green, red, and blue).

These sites account for the majority of the erbium fluorescence. One of them, which we call "P" (green), shows a two-fold larger number of crystal fields than possible

for single erbium dopants in the absence of a magnetic field. We therefore attribute these lines to Erbium precipitates. The mutual coupling of emitters in these sites may lead to coherence times that are too short for quantum applications.

In contrast, we observe only seven CF levels in the excited state for the two other main sites, as expected for erbium dopants in low-symmetry sites [20]. We call these sites "A" (blue, 1537.78(2) nm) and "B" (red, 1536.07(2) nm). They show a large splitting between the lowest two CF levels in both ground and excited state — considerably larger than in all previously investigated erbium hosts, including Y_2SiO_5 , Y_2O_3 , $\text{Y}_3\text{Al}_5\text{O}_{12}$, LiNbO_3 , YVO_4 and CaWO_4 (see supporting information). Combined with the higher Debye temperature of silicon [4], this can improve the optical coherence at higher temperature, as we will show below.

In addition to the favorable CF splitting, the optical transitions of the newly discovered sites A and B also exhibit a large branching ratio, defined as the fraction of photons emitted on the transition between the lowest CF levels in the ground and optically excited state manifold. This transition is most relevant for quantum applications, as the involved levels cannot relax via phonon emission [20]. By splitting the light emitted into the waveguide into a filtered and an unfiltered optical path with calibrated relative transmission, we measure a branching ratio of 20(5)%, comparable to other erbium hosts (see supporting information). The uncertainty reflects the estimated wavelength dependent loss at the photonic crystal reflector and the fiber-to-chip interface.

For all measured sites, we observe narrow inhomogeneous lines (Fig. 2a). We attribute their double-peak structure with a separation of 0.32(1) GHz (green), 0.65(1) GHz (site A, blue) and 0.36(1) GHz (site B, red) to the two isotopes ^{167}Er and ^{170}Er , which have been implanted with equal dose. The two peaks have an equal full-width-at-half-maximum of 0.23(1) (green), 0.40(1) (blue), and 0.44(1) GHz (red), again improving compared to most other hosts (see supporting information) and to our earlier work [11].

The observation of such narrow resonances indicates a homogeneous strain in the silicon device layer, as well as dopant integration at well-defined lattice sites. This constitutes a key step towards quantum-controlled applications of erbium-doped silicon. It is not only beneficial for achieving a sufficient optical depth for on-chip quantum memories, but also shows that our implantation and annealing procedure does not substantially damage the crystal structure, which would lead to a large inhomogeneous broadening and a short coherence time of embedded rare-earth dopants [20].

Similar to other host crystals, the remaining inhomogeneous broadening is attributed to random strain fields in the waveguide that are caused by the different thermal expansion coefficients of Si and SiO_2 , by small residual

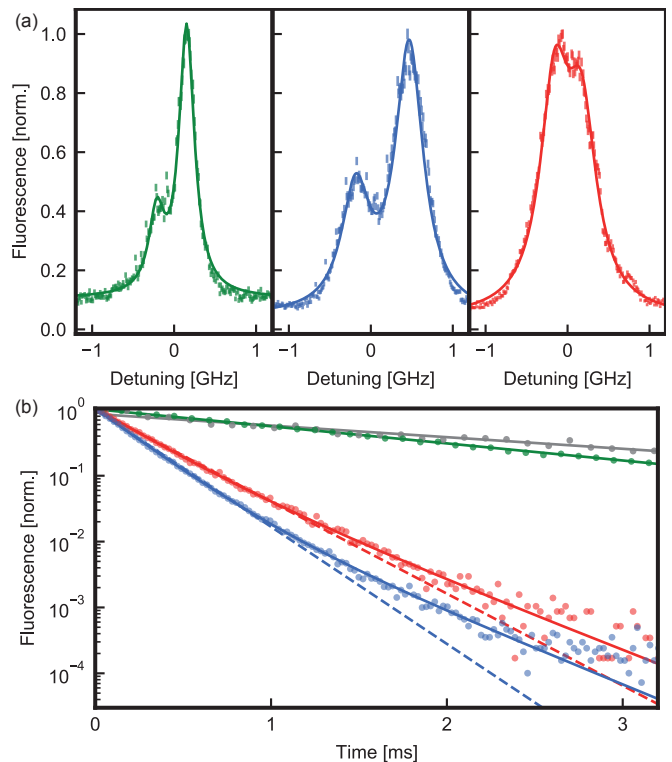


FIG. 2. **Inhomogeneous linewidth and optical lifetime.** a) The resonant fluorescence after excitation laser pulses of different wavelength is detected. The observed lines are well-fit by two Lorentzians with equal FWHM, which we attribute to the two implanted isotopes. Around the resonances, we observe a broader fluorescence background. b) This background decays on a timescale of 2.47(6) ms (grey), consistent with earlier observations under off-resonant excitation [19]. In contrast, upon resonant excitation of a higher CF level, we observe faster decays on the filtered lowest CF transition: 1.67(1) ms (site P, green), 0.244(1) ms (site A, blue) and 0.311(1) ms (site B, red). Instead of a single exponential decay (dashed), at longer times the curves are better fit by a bi-exponential curve (solid), which is explained by the variation of the photonic density of states at different dopant positions and orientations in the waveguide (see supporting information).

amounts of oxygen and other impurities, and finally by the mixed isotopic composition of the crystal. We expect that similar to other emitters in silicon, these sources can be largely eliminated in optimized samples [9], opening exciting prospects for ultra-narrow optical lines in nanofabricated waveguide and resonator structures.

In addition to the large CF splitting and the narrow inhomogeneous broadening, the sites discovered in this work have another advantage: They exhibit comparably fast optical transitions. In Fig. 2b, we show the temporal decay of the fluorescence after the excitation laser is switched off. While the measured lifetime of the background (2.47(6) ms, grey) is in agreement with earlier observations in erbium-doped silicon [19], the other sites

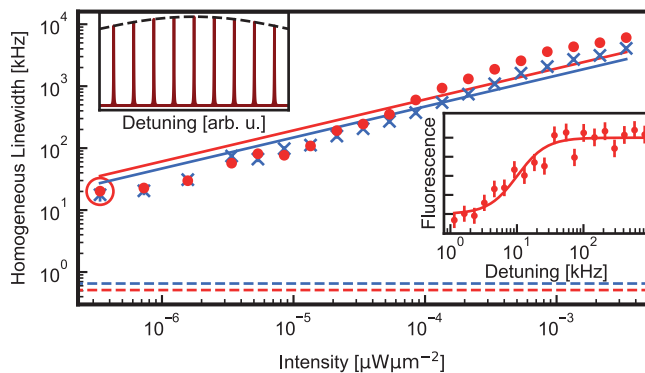


FIG. 3. **Homogeneous linewidth measurement.** Top left inset: Measurement scheme. The laser is modulated to generate a comb of up to 27 lines with equal separation and amplitude, exciting many subensembles (red) within the inhomogeneous line of the dopants (dashed). When the modulation frequency is smaller than the linewidth of the subensembles, saturation leads to a signal decrease (right inset), which is well-fit by Lorentzian curves (red solid) with FWHM down to 17(3) kHz for site A (blue), and 20(3) kHz for site B (red). The extracted linewidth (main graph, red and blue data) exhibits a \sqrt{I} scaling (lines) down to the lowest intensity that provides sufficient signal-to-noise (red circle, inset). This indicates that the measured linewidth is determined by power broadening and thus constitutes an upper bound to the homogeneous linewidth of erbium dopants in the investigated nanophotonic silicon waveguides.

decay much faster, about tenfold for site A and B. Thus, we infer that both sites have strong optical transitions. When using single dopants as qubits, the faster decay results in a significant speedup of single-photon generation and other operations, e.g. more than 50-fold when compared to the commonly used host material YSO [16, 17]. If desired, the lifetime can be further reduced by integrating the erbium emitters into Fabry-Perot [16] or photonic crystal [17] resonators. But even in the absence of such enhancement, the observed decay times of site A and B are faster than the time it takes light to travel 100 km along an optical fiber. Thus, the entanglement rate in global quantum networks based on individual emitters would not be limited by the photon temporal length, but by the signalling time.

To use erbium-doped silicon for quantum applications, the coherence of the optical transition is paramount [3]. We therefore characterize the homogeneous linewidth via transient spectral hole burning [11]. Our measurement technique is based on the observation that the fluorescence signal S increases nonlinearly with the laser intensity I applied at a single frequency, $S \propto \sqrt{I}$, because of saturation. We therefore modulate the input laser field with three concatenated electro-optical modulators in order to apply up to 27 laser fields of about the same intensity I . The fields have an equidistant frequency separation within the inhomogeneous linewidth, exciting dif-

ferent erbium subensembles as shown in the top left inset of Fig. 3.

If the detuning of the laser fields is larger than the ensemble linewidth, their simultaneous irradiation will lead to a 27-fold increase of the fluorescence compared to that of a single field. If, however, the detuning is small, or zero, the fluorescence will only increase by a factor of $\sqrt{27}$ owing to power broadening. Thus, using excitation pulses of 0.15 ms duration and scanning the modulation frequency, we can measure the ensemble linewidth on the timescale of the radiative lifetime. Between repetitions, the laser frequency is shifted to avoid effects of persistent spectral hole burning (see supporting information).

The data is fit with inverted Lorentzian curves, resulting in homogeneous linewidths down to 17(3) kHz, as shown in the right inset. The measured value is an ensemble average; it is limited by power broadening and therefore constitutes an upper bound. This can be seen from the increase of the linewidth with excitation pulse power (main panel), which follows a square-root dependence (solid lines) up to the lowest powers that still give a detectable signal. Thus, the measured homogeneous linewidth is among the narrowest spectral features measured in nanostructured material so far [22], and approaches the lifetime limit of 0.5 kHz.

Still, similar to all other solid-state quantum emitters [4] — including erbium in other hosts [20, 22] — we expect to observe spectral diffusion of a few MHz on longer timescales, caused by the nuclear spin bath and by charge traps at the waveguide interface. Avoiding the former is possible via isotopically purified ^{28}Si , while the latter can be reduced via waveguides or resonators with larger dimensions [16], by suited surface termination (e.g. by hydrogenation), and by charge-trap depletion in strong electric fields [23].

In addition to the fast radiative decay, we expect that the sites A and B keep their coherence when increasing the temperature beyond 2 K. The reason is that both the CF separation and the Debye temperature in silicon, which determine the Orbach and Raman relaxation time, are considerably larger than in other hosts for erbium dopants (see supplement). To investigate this, we increase the sample temperature with a resistive heater and measure the homogeneous linewidth. The result is shown in Fig. 4. For the precipitate site (inset, green), the small separation of the CF levels entails a linewidth of ~ 10 MHz at 2 K, which further increases with temperature. In contrast, we find that the measured value for the two preferred sites A (blue, main graph) and B (red, inset) is constant at low temperature, and only increased beyond the limit of our measurement setup above ~ 10 K. For several settings of the optical intensity, the temperature dependence is well fit by an Orbach process, in which the exponent is determined by the independently measured crystal field splittings. Thus, only the Orbach coefficient of $0.35(10) \text{ s}^{-1} \text{ K}^{-3}$ (site B: $0.31(10) \text{ s}^{-1} \text{ K}^{-3}$)

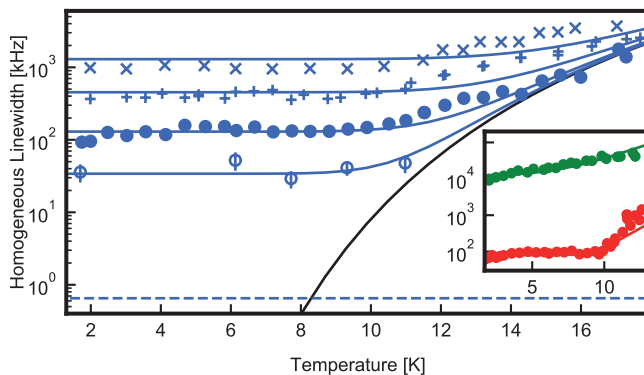


FIG. 4. **Temperature dependence.** The temperature of the sample is changed with a resistive heater and the homogeneous linewidth is determined by transient spectral hole burning. For site A (main panel, blue) and several input powers (different symbols), the linewidth increase with temperature is well explained by Orbach relaxation of the spin levels (blue fit curves). From the Orbach coefficient, in the absence of power broadening (black) we expect that lifetime-limited linewidth (blue dashed) may be observed below ~ 8 K. While site B shows similar temperature dependence (inset, red), the other bright site (green) exhibits much broader lines even at 2 K, owing to its smaller CF level separation.

and the power-broadened linewidth are free parameters in the depicted fit curves.

In the apparent absence of Raman decoherence, the determined Orbach coefficients enable negligible decoherence of the optical transition and second-long lifetimes of the electronic spin already at 4 K, i.e. in a temperature range that is conveniently accessible with dry ^4He cryostats. This is a huge advantage with respect to other emitters in silicon that are broadened to 0.2 GHz at this temperature [15].

In summary, we have observed exceptional optical properties of erbium dopants in silicon nanophotonic waveguides. In contrast to other emitters in silicon [9, 10, 12, 14, 15], their weak coupling to phonons avoids non-radiative decay, phonon-sideband-emission, and thermal broadening even at temperatures around 4K. Compared to erbium in other nanostructured materials [17, 20, 24], we observe much faster optical transitions, smaller inhomogeneous broadening, and a remarkably narrow homogeneous linewidth.

Longer waveguides, or waveguides with larger dopant concentration, should enable long-lived, chip-based quantum memories in robust, cost-effective, and multiplexed devices. In this context, our measurements set a lower bound on the ground-state electron spin lifetime of 0.02ms at 8 K. At lower temperature, exponentially longer lifetimes are expected. At the used concentration, dynamical decoupling can thus give access [25] to quantum memories with long storage time. Alternatively, the large CF splitting of the observed erbium sites entails that second-long hyperfine coherence should be achiev-

able in large magnetic fields [26].

While we have used silicon with natural isotope abundance, isotopic purification is possible even at wafer-scale [7]. This may reduce the detrimental effect of superhyperfine couplings on the coherence, and open exciting prospects for ultra-narrow optical linewidths [9] in the telecom C-band. This would help the implementation of efficient schemes for microwave-to-telecom conversion [27] in a silicon-based platform, which is compatible and routinely used with superconducting qubits.

Finally, single dopants may be resolved by integration into photonic crystal [17] or Fabry-Perot [16] resonators. With the low loss observed in our material, we have realized resonators with a mode volume below a cubic wavelength and a quality factor of $Q > 5 \cdot 10^4$. Further improvement of the latter [28] or further reduction of the former [29], both recently demonstrated in undoped silicon, may then allow for unprecedented Purcell enhancement by six orders of magnitude while preserving the unique potential of frequency-domain multiplexing [17] within a well-controlled ensemble of emitters. This opens promising perspectives for the implementation of cavity-based quantum networks [2, 3] and distributed quantum information processors in a scalable photonic platform.

ACKNOWLEDGEMENTS

We thank Manuel Müller and Stephan Geprägs for assistance with the XRD measurements. This project received funding from the European Research Council (ERC) under the European Union’s Horizon 2020 research and innovation programme (grant agreement No 757772), and from the Deutsche Forschungsgemeinschaft (DFG, German Research Foundation) under Germany’s Excellence Strategy - EXC-2111 - 390814868 and via the project RE 3967/1.

* L.W. and A.G. contributed equally to this work.

† andreas.reiserer@mpq.mpg.de

- [1] Vandersypen, L. M. K. *et al.* Interfacing spin qubits in quantum dots and donors—hot, dense, and coherent. *npj Quantum Inf.* **3**, 1–10 (2017).
- [2] Reiserer, A. & Rempe, G. Cavity-based quantum networks with single atoms and optical photons. *Rev. Mod. Phys.* **87**, 1379–1418 (2015).
- [3] Ruf, M., Wan, N. H., Choi, H., Englund, D. & Hanson, R. Quantum networks based on color centers in diamond. *arXiv:2105.04341* (2021).
- [4] Wolfowicz, G. *et al.* Quantum guidelines for solid-state spin defects. *Nat. Rev. Mater.* 1–20 (2021).
- [5] Vivien, L. & Pavesi, L. *Handbook of Silicon Photonics* (Taylor & Francis, 2013).

- [6] Arrazola, J. M. *et al.* Quantum circuits with many photons on a programmable nanophotonic chip. *Nature* **591**, 54–60 (2021).
- [7] Mazzocchi, V. *et al.* 99.992% Si-28 CVD-grown epilayer on 300 mm substrates for large scale integration of silicon spin qubits. *Journal of Crystal Growth* **509**, 1–7 (2019).
- [8] Saedi, K. *et al.* Room-Temperature Quantum Bit Storage Exceeding 39 Minutes Using Ionized Donors in Silicon-28. *Science* **342**, 830–833 (2013).
- [9] Chartrand, C. *et al.* Highly enriched Si-28 reveals remarkable optical linewidths and fine structure for well-known damage centers. *Phys. Rev. B* **98**, 195201 (2018).
- [10] Morse, K. J. *et al.* A photonic platform for donor spin qubits in silicon. *Sci. Adv.* **3**, e1700930 (2017).
- [11] Weiss, L., Gritsch, A., Merkel, B. & Reiserer, A. Erbium dopants in nanophotonic silicon waveguides. *Optica* **8**, 40–41 (2021).
- [12] Durand, A. *et al.* Broad Diversity of Near-Infrared Single-Photon Emitters in Silicon. *Phys. Rev. Lett.* **126**, 083602 (2021).
- [13] Yin, C. *et al.* Optical addressing of an individual erbium ion in silicon. *Nature* **497**, 91–94 (2013).
- [14] Redjem, W. *et al.* Single artificial atoms in silicon emitting at telecom wavelengths. *Nature Electronics* **3**, 738–743 (2020).
- [15] Kurkjian, A. T. K. *et al.* Optical observation of single spins in silicon. *arXiv:2103.07580* (2021).
- [16] Merkel, B., Ulanowski, A. & Reiserer, A. Coherent and Purcell-Enhanced Emission from Erbium Dopants in a Cryogenic High-Q Resonator. *Phys. Rev. X* **10**, 041025 (2020).
- [17] Chen, S., Raha, M., Phenicie, C. M., Ourari, S. & Thompson, J. D. Parallel single-shot measurement and coherent control of solid-state spins below the diffraction limit. *Science* **370**, 592–595 (2020).
- [18] Gad, M. A., Evans-Freeman, J. H., Cinosi, N. & Sarma, J. Loss measurements of ER-doped silicon-on-insulator waveguides. *Materials Science and Engineering: B* **105**, 79–82 (2003).
- [19] Vinh, N. Q., Ha, N. N. & Gregorkiewicz, T. Photonic Properties of Er-Doped Crystalline Silicon. *Proceedings of the IEEE* **97**, 1269–1283 (2009).
- [20] Liu, G. & Jacquier, B. (eds.) *Spectroscopic Properties of Rare Earths in Optical Materials* (Springer-Verlag, Berlin Heidelberg, 2005).
- [21] Zhang, Q. *et al.* Single Rare-Earth Ions as Atomic-Scale Probes in Ultrascaled Transistors. *Nano Lett.* **19**, 5025–5030 (2019).
- [22] Zhong, T. & Goldner, P. Emerging rare-earth doped material platforms for quantum nanophotonics. *Nanophotonics* **8**, 2003–2015 (2019).
- [23] Anderson, C. P. *et al.* Electrical and optical control of single spins integrated in scalable semiconductor devices. *Science* **366**, 1225–1230 (2019).
- [24] Craiciu, I. *et al.* Multifunctional on-chip storage at telecommunication wavelength for quantum networks. *Optica* **8**, 114–121 (2021).
- [25] Merkel, B., Cova Fariña, P. & Reiserer, A. Dynamical Decoupling of Spin Ensembles with Strong Anisotropic Interactions. *Phys. Rev. Lett.* **127**, 030501 (2021).
- [26] Rančić, M., Hedges, M. P., Ahlefeldt, R. L. & Sellars, M. J. Coherence time of over a second in a telecom-compatible quantum memory storage material. *Nat. Phys.* **14**, 50–54 (2018).
- [27] O’Brien, C., Lauk, N., Blum, S., Morigi, G. & Fleischhauer, M. Interfacing Superconducting Qubits and Telecom Photons via a Rare-Earth-Doped Crystal. *Phys. Rev. Lett.* **113**, 063603 (2014).
- [28] Asano, T. & Noda, S. Photonic Crystal Devices in Silicon Photonics. *Proceedings of the IEEE* **106**, 2183–2195 (2018).
- [29] Hu, S. *et al.* Experimental realization of deep-subwavelength confinement in dielectric optical resonators. *Science Advances* **4**, eaat2355 (2018).